Extremely Correlated Fermi-Liquid Description of Normal-State ARPES in Cuprates

G.-H. Gweon,[1,*] B. S. Shastry,[1,†] and G. D. Gu[2]

[1]Physics Department, University of California, Santa Cruz, California 95064, USA

[2]Condensed Matter Physics and Materials Science Department, Brookhaven National Laboratory, Upton, New York 11973, USA

(Received 13 April 2011; published 29 July 2011)

The normal-state single particle spectral function of the high temperature superconducting cuprates, measured by the angle-resolved photoelectron spectroscopy (ARPES), has been considered both anomalous and crucial to understand. Here, we report an unprecedented success of the new extremely correlated Fermi liquid theory by one of us [B. S. Shastry, Phys. Rev. Lett. **107**, 056403 (2011)] to describe both laser and conventional synchrotron ARPES data (nodal cut at optimal doping) on $Bi_2Sr_2CaCu_2O_{8+\delta}$ and synchrotron data on $La_{1.85}Sr_{0.15}CuO_4$. It fits all data sets with the same physical parameter values, satisfies the particle sum rule and successfully addresses two widely discussed kink anomalies in the dispersion.

DOI: 10.1103/PhysRevLett.107.056404 PACS numbers: 71.10.Ay, 74.25.Jb, 74.72.Gh, 79.60.−i

Angle resolved photoelectron spectroscopy (ARPES) was the first probe to provide a detailed view of the anomalous nature of high temperature cuprate superconductors, discovering unexpectedly broad spectra with intense and asymmetric tails that have remained an enduring mystery for the last two decades. Conventional data taken with high energy ($\gtrsim 15$ eV) photons from synchrotron light sources have recently been supplemented with laser ARPES data [1,2] from lower energy (6 or 7 eV) sources. The latter show considerably sharper features near the Fermi energy. A drastic possibility to account for this distinction is that the sudden approximation could break down for the smaller photon energies used in laser ARPES [3].

An important unanswered question is whether the results of the two spectroscopies could be reconciled in a single theoretical framework that does not abandon the sudden approximation. More broadly, can we understand the wide variety of observed lines shapes in a theoretical framework with a sound microscopic basis and a single set of parameters?

In this Letter, we confront a recent theory of extremely correlated Fermi liquids (ECFL) proposed by Shastry [4] with the above challenge. The new formalism is complex and requires considerable further effort to yield numerical results in low dimensions. In the limit of high enough dimensions, however, a remarkably simple expression for the Green's function emerges; it is significantly different from the standard Fermi-liquid Dyson form, while satisfying the usual sum rules. We use this simple version of ECFL Green's function in this Letter, motivated by the attractive spectral shapes produced with very few parameters [4]. In this Letter we show that already the simplest version of the ECFL theory, with very few parameters, is very successful in detailed fitting of a wide variety of normal-state cuprate ARPES line shapes. Interesting predictions are made for the higher temperature spectral line skew.

Our focus in this Letter is on the data of optimally doped $Bi_2Sr_2CaCu_2O_{8+\delta}$ (Bi2212) and $La_{1.85}Sr_{0.15}CuO_4$ (LSCO) superconductors in the normal state, taken with $\vec{k}$ along the nodal direction connecting (0, 0) to $(\pi/a, \pi/a)$. Most of the data is taken from the published literature, while some original data are also presented (Bi2212 data in Figs. 4 and 5). Our sample is an optimally doped Bi2212 ($T_c = 91$ K), grown by the floating zone method at the Brookhaven National Laboratory (BNL), and was measured at the Stanford Synchrotron Radiation Lightsource (SSRL) beam line 5 − 4 using 25 eV photons. The resolutions are 15 meV (energy) and 0.3° (angle).

Line shape model.—The ECFL spectral function is given as a product of an auxiliary Fermi-liquid (AFL) spectral function $A_{\mathrm{FL}}(\vec{k}, \omega)$ and a second frequency dependent "caparison" factor [4,5]:

$$A(\vec{k}, \omega) = A_{\mathrm{FL}}(\vec{k}, \omega)\left(1 - \frac{n}{2} + \frac{n^2}{4} \cdot \frac{\xi_{\vec{k}} - \omega}{\Delta_0}\right)_+, \quad (1)$$

where n is the number of electrons per CuO_2 unit cell, $(X)_+ \equiv \max(X, 0)$, $\xi_{\vec{k}} = (1 - \frac{n}{2})\varepsilon(\vec{k})$, where $\varepsilon(\vec{k})$ is the bare one-electron band dispersion (see later). Here, $A_{\mathrm{FL}}(\vec{k}, \omega) = \frac{1}{\pi}\mathrm{Im}\frac{1}{\omega - \xi_{\vec{k}} - \Phi(\omega)}$ with

$$\mathrm{Im}\,\Phi(\omega) = \frac{\omega^2 + \tau^2}{\Omega_0}\exp\left(-\frac{\omega^2 + \tau^2}{\omega_0^2}\right) + \eta, \quad (2)$$

where $\tau = \pi k_B T$, T is the temperature, and ω is to be understood as $\omega - i0^+$. Here, ω_0 is the AFL energy scale (i.e., high ω cutoff), and Ω_0 governs the lifetime, and, by causality, the quasiparticle weight (i.e., the wave function renormalization) of the AFL, $Z_{\mathrm{FL}} = (1 + \frac{\omega_0}{\sqrt{\pi}\Omega_0})^{-1}$, as identified from $\mathrm{Re}\Phi$ [6].

The ECFL energy scale Δ_0 measures the "average intrinsic inelasticity" of the AFL. It is given [4] as

$$\Delta_0 = \int_{-\infty}^{\infty} d\omega f(\omega)\langle A_{FL}(\vec{k}, \omega)(\xi_{\vec{k}} - \omega)\rangle_{BZ}, \qquad (3)$$

where $\langle\cdot\rangle_{BZ}$ denotes averaging over the first Brillouin zone.

The parameters that enter this description are now listed. The "primary parameters" defining the ECFL fit consist of the dispersion $\xi_{\vec{k}}$ taken from band theory, the density n, temperature T, and the AFL parameters Δ_0, ω_0, $Z_{\rm FL}$, Ω_0. Of the last four parameters, only two are free parameters. For instance, ω_0 and $Z_{\rm FL}$ can be taken as free parameters, and Ω_0 and Δ_0 can be calculated using the equation for $Z_{\rm FL}$ and Eq. (3), respectively.

The parameter η in Eq. (2) is an additional "secondary parameter" [7] with respect to the ECFL theory [4]. Its origin is in impurity scattering as argued in [8], and additionally, in scattering with surface imperfections. Our fits determine $\eta \approx 0.03$ eV for laser ARPES and $\eta \approx 0.15$ eV for conventional ARPES. Greater penetration depth in laser ARPES suggests that it should be less sensitive to surface imperfections, thereby yielding a smaller η. We therefore propose that this parameter summarizes the effective sample quality in different experiments. The difference in line shapes arising from these values of η is demonstrated in Figs. 1(b) and 1(c).

Our strategy is to fix a common set of intrinsic parameters for all the materials, and allow η to be determined separately for each class of data. The most time consuming part is the calculation of Δ_0, the results of which are summarized in Fig. 1(a).

In our line shape analysis (i) we first set $n = 0.85$, corresponding to the optimal doping. (ii) Here $\xi_{\vec{k}}$ is taken to be the unrenormalized band dispersion, taken from the literature [9], and then scaled to fit the observed occupied band width, 1.5 eV, of the Bi2212 ARPES result [10,11]. (iii) We choose $Z_{\rm FL} = 1/3$, to account for the dispersion renormalization due to the high energy kink [10,12], which in this theory is caused by the energy scale ω_0 (cf. Fig. 5). (iv) Finally, in all simulations, we include the finite energy resolution effect and the finite angle resolution effect as a combined Gaussian broadening (10 meV FWHM for laser ARPES and 25 meV FWHM for conventional ARPES) in energy [13].

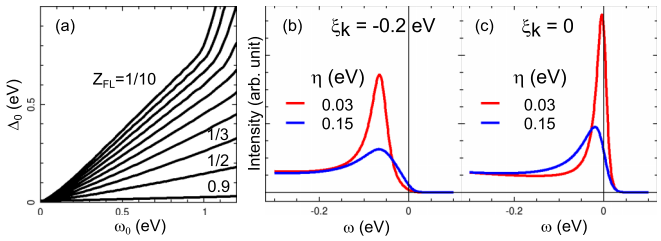

FIG. 1 (color online). (a) Δ_0 as a function of ω_0 for various $Z_{\rm FL}$. Other primary ECFL parameter values are $n = 0.85$, $T = 100$ K, and $\xi_{\vec{k}}$ as described in the text. A small η value, 0.010 eV, was used for this plot, which is used as a "lookup table" during the fit. (b),(c) Examples of the spectral function calculated with different values of the effective sample quality parameter η. See the caption of the next figure for parameter values used. The instrumental energy broadening of 10 meV (FWHM) is included.

Line shape fit for laser ARPES.—Figure 2 shows the fit of the laser ARPES data with the ECFL line shape. These fits were made using a procedure that is somewhat more restrictive than that in the recent work of Casey and Anderson [14,15] invoking the x-ray edge singularity ideas of Doniach-Sunjic, Anderson-Yuval, and Nozieres-de Dominicis [16] (CADS): we are using global, rather than perspectrum, fit parameters. However, our fit is somewhat less restricted than other fits shown in this Letter: here we allow a small variation of $\xi_{\vec{k}}$ as in Ref. [14]. We find an excellent fit quality, at least comparable to CADS [14]. The gray line in panel (a) shows our calculation for $k > k_F$. Our expectation is that, were the data for $k > k_F$ available, we would find a reasonable fit in this k region as well [17], as for other data sets below.

Line shape fit for conventional ARPES.—We find that the magnitude of the parameter ω_0 (0.5 eV) determined from the fit of the sharp laser data works very well also for the conventional ARPES data [18]. Thus, all parameters other than η are fixed, with one small exception in Fig. 4(d), where a slight change in ω_0 produces a much better fit over a larger energy range for LSCO.

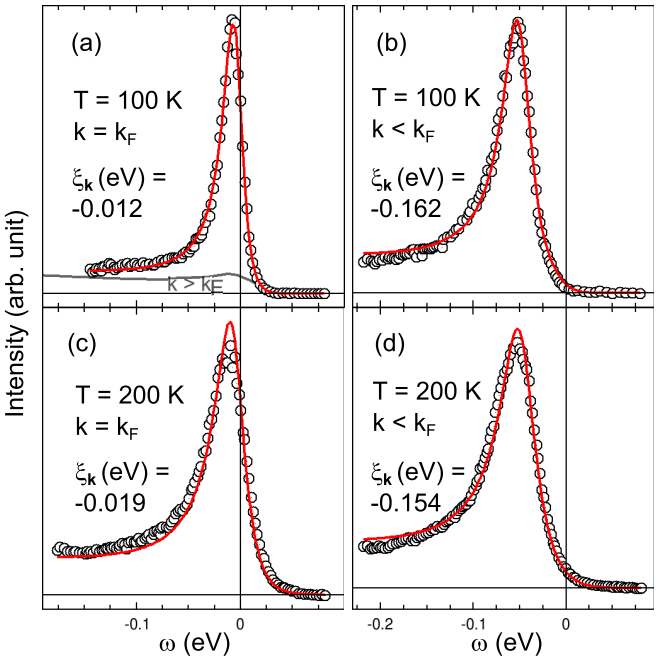

FIG. 2 (color online). Laser ARPES data (symbols, Bi2212) from Ref. [14] fit with the ECFL line shape (red lines). The free parameters of the fit were ω_0 (0.5 eV), η (0.032 eV), and $\xi_{\vec{k}}$ (shown). Fixed parameters: n (0.85), $Z_{\rm FL}$ (1/3). Derived parameters: Δ_0 (0.12 eV), Ω_0 (0.14 eV). Other than η and $\xi_{\vec{k}}$, the same parameters are used elsewhere in the Letter. In (a), the gray line corresponds to the theoretical curve with $\xi_{\vec{k}} = 0.15$ eV.

Figure 3 shows our fit of the data in Ref. [19] with a single free parameter η. The amount of the "extrinsic background" in ARPES is an issue of importance [20–22], especially when analyzing the conventional ARPES data. Here we fit the bg subtracted data, as well as the raw data (panel *d*). For subtracting the background, we use an often-used procedure [22,23] of equating the background to a fraction ("background scaling factor") of the data far beyond the Fermi surface crossing ($k = k_{10}$ for this data set). The background scaling factor, $1/2$ for this figure, is determined to be the maximum value for which the resulting intensity is not negative. As shown in the panel (d), the ECFL fit remains good by adjusting η, whether or not the extrinsic background is subtracted. In contrast, we find that the CADS theory, notwithstanding its notable successes [14,15], cannot cope with even the background subtracted data [Fig. 3(e)], giving too steep a fall off towards the left. Likewise, the MFL fits [8,24] have been shown to compare well with the data only after substantial background subtraction [23,25].

Our own data on Bi2212 data, taken at T_c and well above T_c, covering a similar temperature range as the laser data of Fig. 2, can be fit equally well with the same background subtraction procedure, i.e., with the background scaling factor $(1/2)$, as shown in Fig. 4.

We also find that the data for a lower-T_c cuprate LSCO can be fit very well with the same intrinsic parameters. Here, we shall discuss only the $k = k_F$ data for brevity.

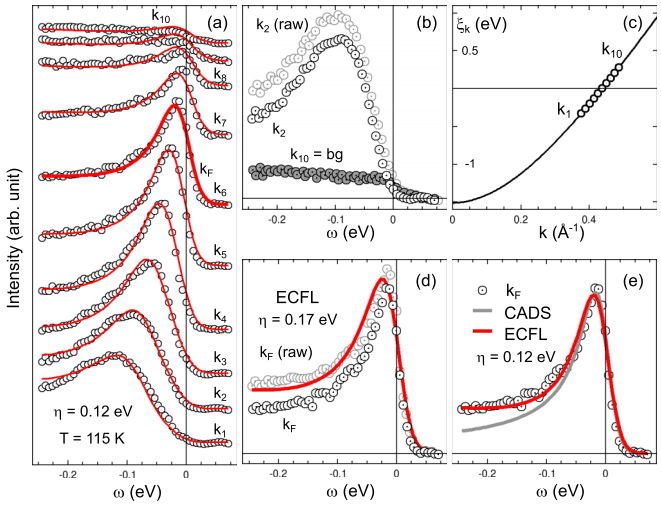

FIG. 3 (color online). Conventional ARPES data (Bi2212) fit with the ECFL line shape. The data are from Ref. [19] (T_c = 90 K). (a) The data (symbols) and the fit (red lines) are shifted vertically by the same amount for ease of view. (b) An example of the raw data and the fit data is shown for k_2. The background (bg) spectrum (see text) was subtracted from each raw data, and the resulting data, shown in (a), are then fit. (c) The fixed $\xi_{\vec{k}}$ parameters used for the fit. Thus, in this figure, η is the only fit parameter (cf. Fig. 2 caption). (d) Raw data at $k = k_F$ fit with a somewhat greater η value. (e) The current fit compared with a fit using the CADS line shape.

In this case, we determine that the background scaling factor be 1. The subtracted background data [26,27] is shown as the gray curve in Fig. 4(c). Given their weak superconductivity features [26,27], these LSCO data are taken to represent the normal-state property even if the temperature is slightly lower than T_c. As for the Bi2212 case, the data can be fit well even without the background subtraction, if a somewhat greater η value (≈ 0.17 eV) is used. It is clear, from Fig. 4(c), that the data at a temperature as low as 25 K can be fit very well with the ECFL line shape. In addition, in working with LSCO line shapes, we noticed a steady and rapid rise in intensity beyond $-\omega = 0.25$ eV, a behavior different from that of Bi2212. We leave the full discussion of this nonuniversal behavior for future work. However, we find it exceptional that the current theory is able to describe the line shape of LSCO up to very high energy, as shown in Fig. 4(d).

Kinks in the spectra.—The two independent energy scales ω_0 and Δ_0 are determined from our fit as ~0.5 eV and ~0.1 eV. These are natural candidates for the two main dispersion anomalies in the cuprates [12,28] as in Fig. 5. Well-defined energy distribution curve (EDC: intensity curve at a fixed $\vec{k}$ value) peaks disappear in a wide energy from ~0.3 eV to ~1 eV, as observed experimentally for the high energy kink [10,12]. As this feature

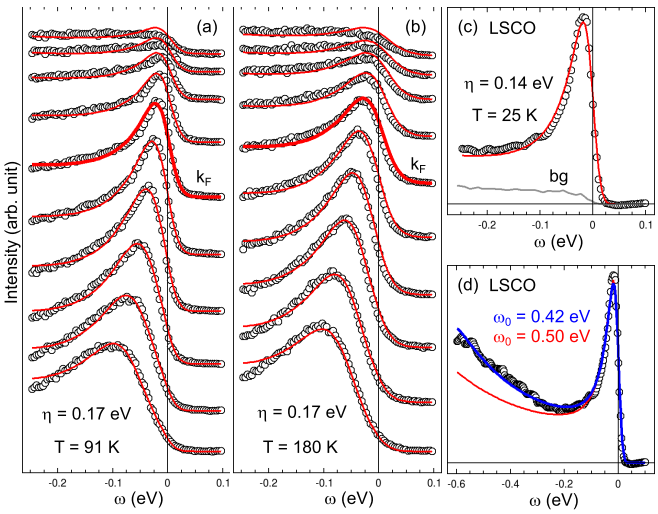

FIG. 4 (color online). Conventional ARPES data, including our own (a),(b), fit with the ECFL line shape. The procedure used to fit these data are identical with those of the previous figure, i.e., a fit with a single free parameter η, with (d) being a single exception. (a),(b), Optimally doped Bi2212 (T_c = 91 K). (c) Optimally doped LSCO data [26,27]. (d) A test fit up to 0.6 eV for the LSCO data with a small change to ω_0 for the same data as in (c) but over a wider energy range. By changing ω_0 slightly from 0.50 to 0.42 eV, we see that an excellent fit up to 0.6 eV is found. The LSCO data, as far as we are aware, is fit only by the ECFL theory, since an energy dependence rising linearly for occupied states occurs naturally and uniquely in the ECFL spectral function.

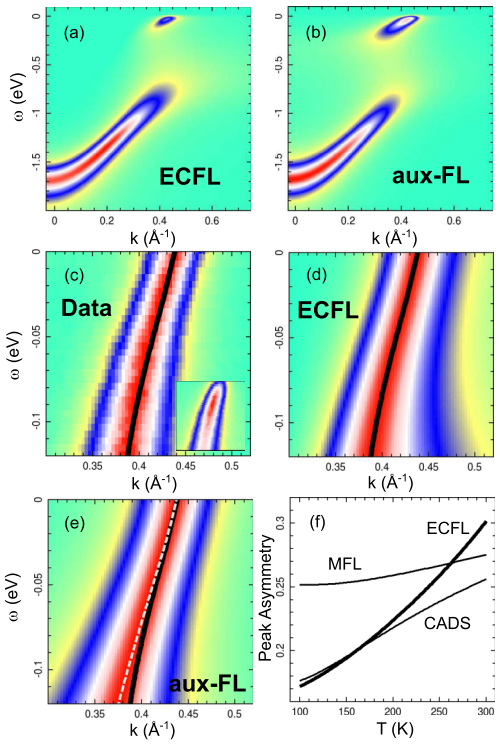

FIG. 5 (color online). Image plots of the spectral function for (a) the ECFL theory ($\eta = 0.17$ eV), and (b) that of the auxiliary FL. (c) The data of Fig. 4(a) before (inset) and after (main) MDC normalization, by which each MDC is scaled and shifted to have minimum 0 (green) and maxmimum 1 (red). Blue corresponds to 1/2. (d) The near-E_F part of the ECFL spectral function of (a), after MDC-normalization with MDC peak positions traced by black line. The black line in (c) is from (d). (e) The near-E_F part of the AFL spectral function of (b) after MDC-normalization. The MDC peak positions are traced by gray dashed line, while the black line is from (d). The bending such as shown by the black line here is commonly referred to as the kink. (f) The temperature dependence of the peak asymmetry compared for three different theories, rising as T^2 for ECFL. Theory parameters for the calculation, apart from T, are taken from the fit of Fig. 2(a) for the ECFL, from the equivalent fit of Ref. [14] for the CADS, and from Ref. [25] for the MFL.

already exists in AFL, it cannot be associated with Δ_0 but rather with ω_0. The (numerical) dynamical mean field theory [29] can already account for this feature as can the present ECFL (analytical) theory.

Turning to the low energy ARPES kink at ~70 meV, Figs. 5(c)–5(e) illustrate the observed weak dispersion anomaly in the normal-state data (c), reproduced in the ECFL theory (d) but not in the AFL theory (e). Here we use a visualization method for momentum distribution curve (MDC: intensity curve at a fixed ω value), an object discussed primarily for low energy kinks. Thus this feature originates from the scale Δ_0, it causes an increased asymmetry and the (blue) shift of the peak to high hole energy, when the third term in the caparison factor $(\frac{n^2}{4}\frac{\xi_{\tilde{k}}-\omega}{\Delta_0})$ of Eq. (1) becomes important. To our knowledge, the ECFL theory is a unique analytical theory that has both these kink features arising from purely electronic (extreme) correlations.

In Fig. 5(f), we show the temperature dependence of the dimensionless peak skew or asymmetry, defined as (HL − HR)/(HL + HR), where HR (HL) is the half-width at half maximum on the right (left) side of the peak. The predicted T-dependent asymmetry, predicted even greater for $\eta \approx 0.15$ eV (synchrotron data; not shown), would be interesting to explore in the future.

Further work is necessary to refine the picture suggested in this Letter. For example, as $-\xi_{\tilde{k}}$ increases, the line shape becomes somewhat too asymmetric. Work is also in progress to apply the theory to two particle response as seen, e.g., in optical conductivity. We have checked that the bubble approximation (conductivity as a product of two G's) shows an agreement in the order of magnitude of the frequency scale and the conductivity.

Conclusions.—We have shown that it is possible to understand both ARPES data sets (laser or conventional) comprehensively, with identical physical parameters. Work going beyond the nodal cut and the optimal doping value is in progress. The theory is very tolerant of the uncertainty in the background subtraction for the conventional ARPES data. Additionally, the theory satisfies the global particle sum rule, and contains two interdependent energy scales (ω_0 and Δ_0) that correspond well to the energy scales of the two kinks. Thus the simplest version of the ECFL theory using a small number of parameters, provides a framework to understand the ARPES line shape data for the normal state of the cuprates: it works extremely well across techniques, samples, and temperatures.

Portions of this research were carried out at the SSRL, a Directorate of SLAC National Accelerator Laboratory and an Office of Science User Facility operated for the U.S. DOE Office of Science by Stanford University, and at the BNL, supported by the U.S. DOE under Grant No. DE-AC02-98CH10886. The work by GHG was supported partially by COR-FRG at UC Santa Cruz. BSS was supported by U.S. DOE under Grant No. FG02-06ER46319.

*gweon@ucsc.edu
†sriram@physics.ucsc.edu

[1] J. D. Koralek *et al.*, Phys. Rev. Lett. **96**, 017005 (2006).
[2] W. Zhang *et al.*, Phys. Rev. Lett. **100**, 107002 (2008).
[3] In the sudden approximation, the ARPES intensity $I(\vec{k}, \omega) = M(\vec{k})A(\vec{k}, \omega)f(\omega)$. Here, $\vec{k}$ is the momentum and $-\omega$ is the energy of the final $N-1$ state (as we set $\hbar = 1$ in this Letter), where N is the number of electrons in the initial state. $A(\vec{k}, \omega) = \mathrm{Im}\, G(\vec{k}, \omega - i0^+)/\pi$ is the single particle spectral function, $M(\vec{k})$ is the dipole matrix element, constant for an EDC, and $f(\omega)$ is the Fermi-Dirac function. At the chemical potential $\omega \equiv 0$.

[4] B. S. Shastry, this issue, Phys. Rev. Lett. **107**, 056403 (2011).
[5] B. S. Shastry, arXiv:1104.2633.
[6] $\mathrm{Re}\Phi(\omega) = -1/(\sqrt{\pi\Omega_0})\exp(-\frac{\tau^2}{\omega_0^2})[\omega_0\omega - 2(\omega^2+\tau^2)D(\frac{\omega}{\omega_0})]$, where $D(x) = (\sqrt{\pi}/2)e^{-x^2}\mathrm{erfi}(x)$ is the Dawson function. $C_\Phi = 1/(\pi\Omega_0)$ and $\omega_c = C_\Phi\omega_0^2$, where C_Φ and ω_c are parameters defined in [4].
[7] By secondary, we mean "intrinsic [i.e., part of $A(\vec{k}, \omega)$] but dependent on the effective sample quality."
[8] E. Abrahams and C. M. Varma, Proc. Natl. Acad. Sci. U.S.A. **97**, 5714 (2000).
[9] R. S. Markiewicz *et al.*, Phys. Rev. B **72**, 054519 (2005).
[10] W. Meevasana *et al.*, Phys. Rev. B **75**, 174506 (2007).
[11] Also, a minor k shift of the theory was necessary (~ 0.02 Å) to match the slightly different k_F values reported in different experiments.
[12] J. Graf *et al.*, Phys. Rev. Lett. **98**, 067004 (2007).
[13] The minor effect of the finite angular resolution, significant only for the conventional ARPES data, can be modeled well by an energy broadening.
[14] P. A. Casey *et al.*, Nature Phys. **4**, 210 (2008).
[15] P. W. Anderson, Nature Phys. **2**, 626 (2006).
[16] S. Doniach and M. Sunjic, J. Phys. C **3**, 285 (1970); P. Nozieres and C. T. De Dominicis, Phys. Rev. **178**, 1097 (1969); G. Yuval and P. W. Anderson, Phys. Rev. B **1**, 1522 (1970).
[17] J. Koralek, Ph.D. thesis, University of Colorado, 2006.
[18] When it is allowed to vary but k independent, it is 0.5 eV within $\pm \sim 10\%$.
[19] A. Kaminski *et al.*, Phys. Rev. Lett. **86**, 1070 (2001).
[20] C. G. Olson *et al.*, Phys. Rev. B **42**, 381 (1990).
[21] G. Gweon, J. W. Allen, and J. D. Denlinger, Phys. Rev. B **68**, 195117 (2003).
[22] A. Kaminski *et al.*, Phys. Rev. B **69**, 212509 (2004).
[23] T. Valla *et al.*, Science **285**, 2110 (1999).
[24] C. M. Varma *et al.*, Phys. Rev. Lett. **63**, 1996 (1989).
[25] A. Kaminski *et al.*, Phys. Rev. B **71**, 014517 (2005).
[26] T. Yoshida *et al.*, J. Phys. Condens. Matter **19**, 125209 (2007).
[27] T. Yoshida, Ph.D. thesis, University of Tokyo, 2001.
[28] A. Lanzara *et al.*, Nature (London) **412**, 510 (2001).
[29] K. Byczuk *et al.*, Nature Phys. **3**, 168 (2007).